Int. J. Electrochem. Sci., 8 **(2013)** 12451 - 12465

International Journal of
ELECTROCHEMICAL
SCIENCE
www.electrochemsci.org

Iron Based Degradable Foam Structures for Potential Orthopedic Applications

Renáta Oriňáková[1*], *Andrej Oriňák*[1], *Lucia Markušová Bučková*[1], *Mária Giretová*[2], *Ľubomír Medvecký*[2], *Evelína Labbanczová*[1], *Miriam Kupková*[2], *Monika Hrubovčáková*[2], *Karol Koval*[2]

[1] Department of Physical Chemistry, Faculty of Science, P.J. Šafárik University, Moyzesova 11, SK-04154 Košice, Slovak Republic, European Union
[2] Institute of Materials Research, Institute of Material Research, Slovak Academy of Science, Watsonova 47, SK-04353 Košice, Slovak Republic, European Union
[*]E-mail: Renata.Orinakova@upjs.sk

Received: 29 July 2013 / *Accepted:* 17 September 2013 / *Published:* 20 October 2013

Iron and iron based alloys have been identified as appropriate biodegradable osteosynthesis material with the ability of bearing high loads for the temporary replacement of bones. They combine high strength at medium corrosion rates. Open cell iron based foams have been manufactured by replication method on the basis of the highly uniform structure of foamed polyurethane by powder metallurgical approach. Bare carbonyl iron samples and samples with addition of carbon nanotubes (CNTs) and magnesium have been tested with respect to their microstructure, their degradation rate, and their cytotoxicity. The electrochemical corrosion behaviour has been studied in Hank's solution and physiological saline solution. Potentiodynamic polarization experiments conducted at 37°C indicated the increased biodegradation rates resulted from porous structure of foam samples. Corrosion rates determined by the Tafel extrapolation method were in the sequence: Fe-Mg, Fe, Fe-CNTs from higher to lower. The cytotoxicity test showed small proliferation of osteoblastic cells incubated on iron based samples.

Keywords: open cell foams, iron, powder metallurgy, corrosion, cytotoxicity

1. INTRODUCTION

Metals, ceramics and polymers are the most commonly used materials in the biomedical field [1, 2]. The degradable biomaterials represent new kind of implants based on biodegradable metals such as magnesium and iron. Biodegradable metal alloys play a key role in the repair or the replacement of bone defects [2, 3]. They can adapt to the human body in which they are implanted and due to their mechanically stability there are able to provide a temporary healing support of diseased tissue or organ

while degrading at a potentially adjustable degradation rate [3, 4, 5]. As bone regeneration increases, the resorbtion of the implant material introduces an augmented load transmission to the bone. A period of 6–18 months is desired for the remodelling process to be completed [3]. Since the stiffness of metals greatly exceed the stiffness of bones the cellular metals with low young's modulus have been proposed to avoid the resulting problems of stress shielding [6, 7, 8]. Cellular metals typically fall within the stiffness range of cancellous bone [9]. Open cell metal foams enable bone cells ingrowth and blood vessels incorporation promoting implant stabilization [3, 6, 10]. In the ideal case, progressive osteointegration on the one hand and degradation of the implant on the other hand, guarantee an optimal adaptation to the corresponding strength state at any time [3].

Iron shows good mechanical properties and relatively long degradation timeframes, which in particular are needed when higher loads should be carried [11]. This plays a major role when cellular materials are used [12]. Recently, pure iron and iron based alloys are believed to be suitable materials for the production of biodegradable stents for cardiovascular surgery [3, 13]. Although the analysis of cytotoxicity of metal ions shows a low biocompatibility [14] the implanted stents were completely resorbed and did not leave any distinctive inflammatory reactions and serum levels in blood investigations [15, 16]. However, the first in vivo studies of pure iron show fairly low corrosion rates [3, 17]. The corrosion of iron could be promoted by various alloying elements.

Mg and its alloys are now viewed as a potential alternative for making scaffold for tissue regeneration application due to combination of their excellent mechanical properties and degradability [18, 19]. Mg is necessary for calcium incorporation into bone, and so the release of Mg ions is expected to be beneficial for bone healing [1, 20, 21]. The cellular magnesium materials have been developed and examined in clinical tests as implant materials in bone surgery [22] and cardiovascular surgery [23]. It was found that even thought this material is highly biocompatible and features excellent osteoconductivity, it corrodes at such a high speed that the newly established bone is not yet able to carry the load necessary.

Carbon is the major alloying element in steels and has different effects on the corrosion properties under different circumstances [24]. Carbon nanotubes (CNTs) have been primary used in nanotechnology, electronics, optics, medicine, and materials science [25, 26]. Currently they are regarded as ideal materials for use in a growing range of applications [27]. In addition to their remarkable physical and electrical properties, CNTs have proven to be highly biocompatible, which has led to their use for biosensing, molecular delivery, electrochemical detection of biological species, and tissue scaffolding [27, 28, 29]. Carbon nanotube based substrates have been shown as suitable scaffold materials for osteoblast proliferation and bone formation [30, 31]. Moreover, the antimicrobial nature of carbon nanotubes has attracted significant attention [32, 33, 34]. Since carbon nanotubes are not biodegradable, they behave like an inert matrix on which cells can proliferate and deposit new living material, which becomes functional normal bone [27].

The aim of the present study was to design implants with an open cell structure as degradable bone replacement material and to study the corrosion properties and cytotoxicity of developed samples. The iron foams were prepared by a powder metallurgical replication route. In order to increase the corrosion rate and biocompatibility, CNTs and Mg as a minority component were used.

The effect of CNTs and Mg addition to the carbonyl iron powder on the microstructure, surface morphology, biodegradation and cytotoxicity has been evaluated in this study.

2. EXPERIMENTAL PART

2.1 Materials preparation

The carbonyl iron powder (CIP) fy BASF (type CC, d50 value 3.8 – 5.3 μm) with composition: 99.5 % Fe, 0.05 % C, 0.01 % N and 0.18 % O was used for the experiments as a starting material.

A reticulated polyurethane sponge (Bulpren S 28133 or Fitren TM 25133) with cell size 1060 – 1600 μm was entirely impregnated by slurry comprising metal particles. In the next step, the template was thermally removed in a tube furnace Aneta 1 for 2 hours at 450 °C in nitrogen atmosphere and finally the debinded metal structure was sintered for 1 hour at 1120 °C in reductive atmosphere (10 % H_2 and 90 % N_2) to produce open cell iron foam.

The samples with addition of CNTs or Mg were prepared by the same procedure from the mixtures of 0.5 wt % of CNTs or Mg and carbonyl iron powder. Mixtures of iron and magnesium were prepared by mixing carbonyl iron and fine 99.8 % pure Mg-powders (Goodfellow GmbH, Germany) with a particle size of 50 μm. Mixtures of iron and CNTs were prepared by mixing carbonyl iron and multi-walled carbon nanotubes (OD < 8 nm; Length 50 μm; Purity > 95 wt %) of Creative Nanotech production.

Since CNTs and Mg are insoluble with iron, the sintering temperatures of Fe-CNTs and Fe-Mg mixtures remained unchanged.

For the cytotoxicity test, powder mixtures were cold pressed at 400 MPa into pellets (Ø 10 mm, h 5 mm) and sintered in the same way as cellular samples.

2.2 Materials characterization

The microstructure of the experimental specimens was observed by a scanning electron microscope (JOEL JSM-7001F, Japan).

The cells on substrates were observed using a fluorescence microscope (Leica DM IL LED, Germany, blue filter).

The specific surface of prepared samples was determined by the BET method. The values of surface area as high as 0.40 m^2/g, 0.48 m^2/g, and 0.30 m^2/g were obtained for bare Fe sample, Fe-CNTs and Fe-Mg sample, respectively.

2.3 Electrochemical measurements

The electrochemical studies were conducted using an Autolab PGSTAT 302N potentiostat, interfaced to a computer. Measurements were carried out by conventional three-electrode system with the Ag/AgCl/KCl (3 mol/l) reference electrode, platinum counter electrode and iron foam sample as

the working electrode. The simulated body liquid electrolyte was Hank's solution with a pH value of 7.4 or 9 g/l NaCl solution with a pH value of 7.2, prepared using laboratory grade chemicals and double distilled water. The composition of the Hank's solution used was: 8 NaCl, 0.4 KCl, 0.14 $CaCl_2$, 0.06 $MgSO_4.7H_2O$, 0.06 $NaH_2PO_4.2H_2O$, 0.35 $NaHCO_3$, 1.00 Glucose, 0.60 KH_2PO_4 and 0.10 $MgCl_2.6H_2O$ (in g/l). Freshly prepared solution was used for each experiment. A constant electrolyte temperature of 37±2°C was maintained using a heating mantle. All the potentiodynamic polarization studies were conducted after stabilization of the free corrosion potential. The potentiodynamic polarization tests were carried out from -1200 mV to +200 mV (vs. Ag/AgCl/KCl (3 mol/l)) at a scanning rate of 0.5 mV/s. The corrosion rate was determined using the Tafel extrapolation method.

2.4 Cytotoxicity test

Each sample was mechanically polished to 600 and then to 1200 grit and cleaned in ethanol. The samples were than cleared of residual corrosion products by immersion in H_3PO_4 (conc.) for 30 s and sterilized in a thermostat at 170°C for 1 hour.

The sterilized samples were placed in a 48-well suspension plate, seeded with $4.0x10^4$ cells in 500 µl of complete medium MEM (Minimum essential medium with Earles balanced salts, 2 mmol/l L-glutamine, 10 % fetal bovine serum and Penicillin + Streptomycin + Amphotericin solution) and cultured at 37°C in 5 % CO_2 and 95 % humidity in incubator. Substrates were evaluated after 3 days of cell seeding. The pure titanium sheet was used as a negative control of cytotoxicity. The acridine orange (AO), (Sigma-Aldrich) was used to stain the MC3T3 cells proliferated on scaffolds. The samples were rinsed with phosphate buffered saline solution (PBS); cells were fixed in 96 % ethanol for 20 minutes and stained with 0.01 % AO solution for 2 minutes in the dark. The cells on substrates were observed using a fluorescence microscope to investigate the cell distribution on the sample surfaces.

3. RESULTS AND DISCUSSION

The purpose of the present study was the investigation of the effect of CNTs and Mg addition as a minor component on the microstructure, cytotoxicity and degradation rate of powder metallurgical carbonyl iron foams with respect to their use as degradable bone implant material with a cellular structure. Selected additives were added in order to enhance the biocompatibility and corrosion rate of iron implants.

3.1 Iron based foams structure

The complete transformation of the open network of the polymer foam template to the metal foam was allowed by replication method.

Figure 1. Carbonyl iron based cellular material prepared by powder metallurgy: Fe (a); Fe-CNTs (b); Fe-Mg (c). Sample diameter is 0.9 - 1 cm and length is 3.5 – 4 cm.

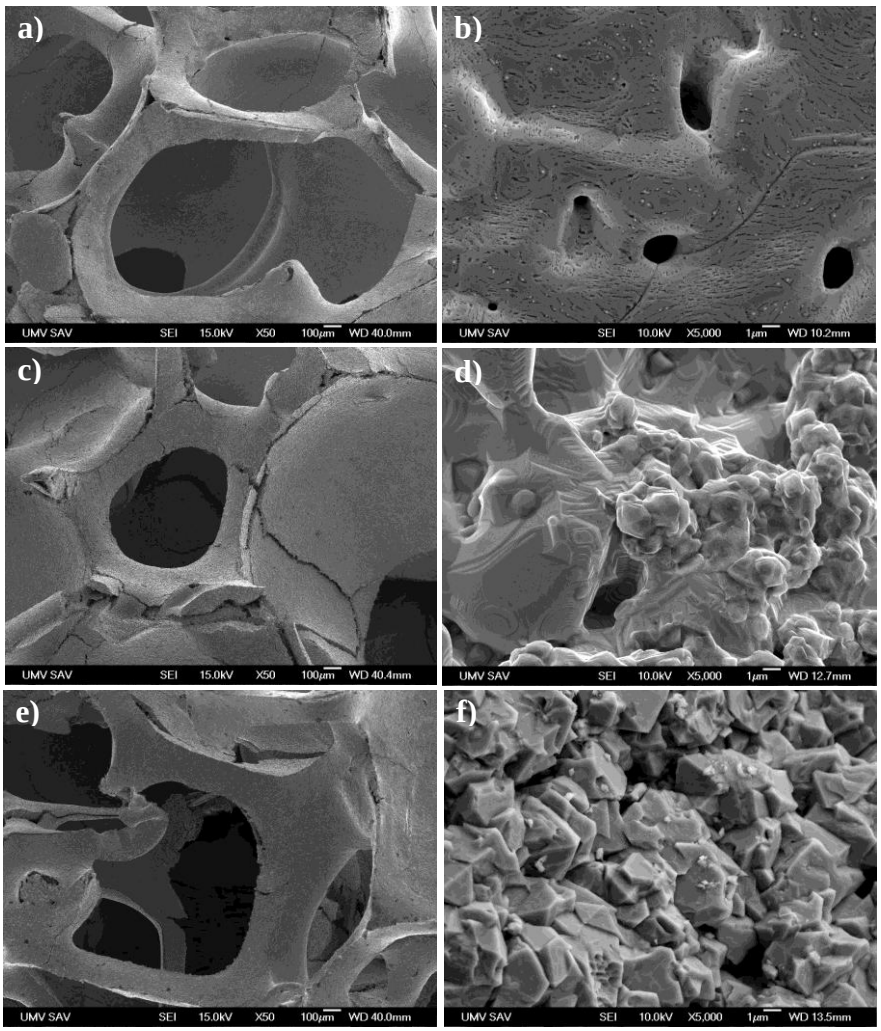

Figure 2. Electron microscopy picture of metal foams prepared by powder metallurgy: Fe (a, b); Fe-CNTs (c, d); Fe-Mg (e, f).

The resulted metal foams closely resemble the original polyurethane sponge structure with hollow struts after the sintering. Figure 1 shows the structure of the prepared high porosity carbonyl iron based open cell sintered foams with cell size between ppi 35-50 and a density of about 24 kg/m^3. The cell size of the polymer templates correlates with diameters of the large cell of approx. 1 mm.

The micrographs of the powder metallurgical samples were prepared in order to analyze the microstructure of different sintered metallic foams. Fig. 2 shows the surface of metallic foams prepared from bare carbonyl iron powder (Fig. 2a, b) and from carbonyl iron powder mixed with CNTs (Fig. 2c, d) or Mg powder (Fig. 2e, f). In microstructures, the high fractions of large almost spherical macropores with size up to 800 μm are clearly visible. The wall thickness between individual macropores is around 200 - 300 μm.

A low number of micropores (size about 5 μm) was found in all samples but spherically shaped micropores were observed in Fe foams contrary to others. The addition of CNTs to carbonyl iron (Fig. 2c, d) leads to an increase in surface roughness, microstructure inhomogeneity, and crack density in the compacts. The noticeable different surface morphology was obtained by sintering of powder samples prepared from mixture of carbonyl iron and Mg. Both the microporosity and roughness rose in this sample and regular pyramidal particles with sharp edges were observed on pore surfaces.

3.2 Electrochemical corrosion behaviour

3.2.1 Hank's solution

Degradation of iron foams in Hank's solution was examined by anodic polarisation curves at 37°C. Five cycles of anodic potentiodynamic polarisation were registered for every sample (Fig. 3). The reproducibility of Tafel plots was good. The corrosion potential (E_{corr}) and corrosion current density (i_{corr}) were calculated from the intersection of the anodic and cathodic Tafel lines extrapolation. All values of E_{corr} and i_{corr} for five cycles are summarized in Table 1. The addition of CNTs and Mg results in a higher (more noble) corrosion potential. This positive shift gives indication about the decreased corrosion susceptibility of iron foams containing additives. The significant shift of corrosion potential to the less negative values for Fe-Mg sample in first cycle could be associated with the existence of the air formed passive surface layer. Saw suggested that magnesium materials exposed to atmospheric conditions develop a thin gray layer on its surface, which is partially protective [35]. Song et al. [36] reported that magnesium forms a magnesium hydroxide film which inhibits direct contact of the magnesium with the solution. This film may also cause the measured corrosion potential to be larger (more noble) than the theoretical value. However, the Fe-Mg samples showed the highest degradation rate. The in-vitro degradation rates in Hank's solution were determined from potentiodynamic polarisation curves. The average corrosion rates are listed in Table 1. Iron mixture with CNTs resulted in lowest degradation rate among the three experimental materials. This is in contrast with results of Cheng et al. [37]. They found that the corrosion potential of Fe-CNT composite prepared by spark plasma sintering in Hank's solution was greatly decreased after the addition of CNT. The addition of CNT (0.5 wt% or 1.0 wt%) in pure iron increased the corrosion current densities compared with pure iron. Furthermore, the corrosion current densities increased with the increasing content of additive phase. The shift of corrosion potential to the less negative values together with decrease in corrosion rate was observed for pure iron samples and samples containing CNTs with increasing number of polarisation cycles. This indicated some inhibition of corrosion by rust layer. Ca/P compounds precipitated on the surface of hydroxide layer from Hank's solution as the corrosion

proceeded [37]. Samples with magnesium displayed an increase in corrosion rate associated with shift of corrosion potential to the more negative values. The passive layer on the foam sample top-surface, which to some extent protected the cellular material, was dissolved during the first cycle of anodic polarisation thereupon in next cycle iron foams showed a higher tendency to corrode. Moreover, Cl^- can penetrate from the rust layer, destruct the structure of the rust layer and react with the substrate metal directly [38, 39]. Since Mg and Fe are not dissoluble, Mg particles may act as local corrosion spots, leading to enhanced intergranular corrosion. As it was reported earlier [35, 37, 39] the active nature of Mg means that galvanic effects are always an issue in Mg-Fe alloys. Mg is more active than Fe, and consequently Mg is the anode and corrodes preferentially. However, the difference in corrosion current densities between the samples is not significant. The corrosion rates calculated from corrosion current densities are of the same order of magnitude, which could correspond to the low content of additive elements.

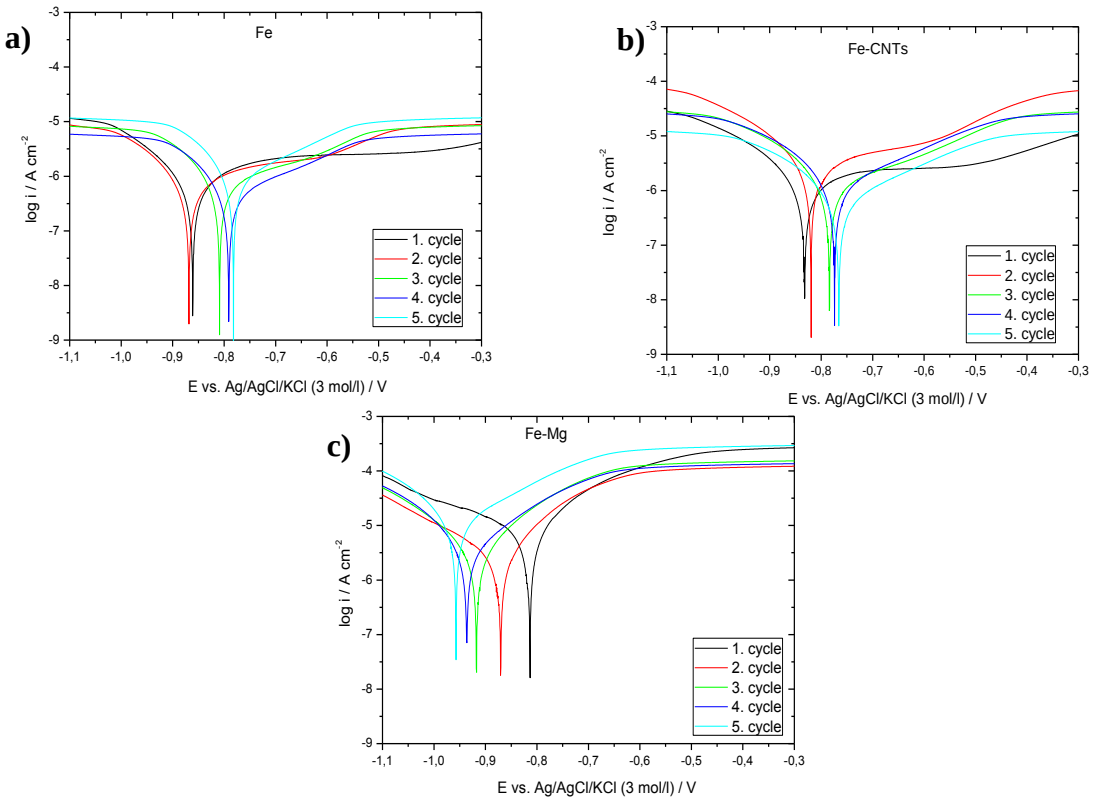

Figure 3. First five cycles of polarization curves of metal foams prepared by powder metallurgical method in Hank's solution at pH 7.4 and 37°C: Fe (a); Fe-CNTs (b); Fe-Mg (c).

The corrosion rates of porous samples are higher than ones reported for nonporous iron based samples [40] which could be assigned to higher surface area, roughness, and penetrable structure of cellular material. The addition of CNTs caused slight decrease in corrosion rate while addition of Mg resulted in moderate increase in degradation rate.

Table 1. Determined values of E_{corr}, i_{corr} and corrosion rates obtained from the potentiodynamic polarization curves in Hank's solution at pH 7.4 and 37°C.

Cycle	E_{corr} (mV)			i_{corr} (μA/cm^2)			Corrosion rate (mm/year)		
	Fe	Fe-CNTs	Fe-Mg	Fe	Fe-CNTs	Fe-Mg	Fe	Fe-CNTs	Fe-Mg
1.	-860.7	-832.5	-812.0	3.492	3.118	3.375	0.972	0.650	0.765
2.	-867.8	-821.1	-870.0	3.435	2.992	4.010	0.715	0.647	0.789
3.	-808.4	-786.3	-915.9	3.420	2.921	4.222	0.702	0.628	0.798
4.	-791.4	-772.5	-933.8	3.357	2.873	4.380	0.695	0.609	0.807
5.	-782.6	-763.2	-959.7	3.290	2.714	4.629	0.678	0.589	0.820

In Fig. 4 the detail of corroded porous material surface after corrosion test are shown. The surface of iron cellular material after corrosion test is more rough and damaged in contrast with surface before corrosion (Fig. 2) and corrosion products can be seen. While the localised corrosion on the surface of bare iron sample and Fe-CNTs was observed, the more uniform corrosion propagation on the whole iron foam surface was detected for sample with addition of Mg. The highest amount of corrosion products together with highest extent of surface damage and more uniform corrosion propagation could be seen for Fe-Mg sample (Fig. 4c). Furthermore, the reduction of interparticle contacts and thus higher fragility of all corroded samples was observed on the lower magnification micrographs.

It was reported by Cheng et al. [37, 41] that the corrosion type of Fe in Hank's solution is localized corrosion. The corrosion mode of Fe-CNT composite turned out to be uniform corrosion instead of localized corrosion. Generally, pits were easily formed in the corrosion of pure iron due to localized acidification beneath the hydroxide layer, where the surface was loose with small micro-pores. For Fe-CNT composite, as second phase uniformly distributed in the iron matrix, widespread galvanic corrosion took place with multiple tiny pits formed and hydroxide products uniformly covered the surfaces, resulting in general corrosion of the material macroscopically [37].

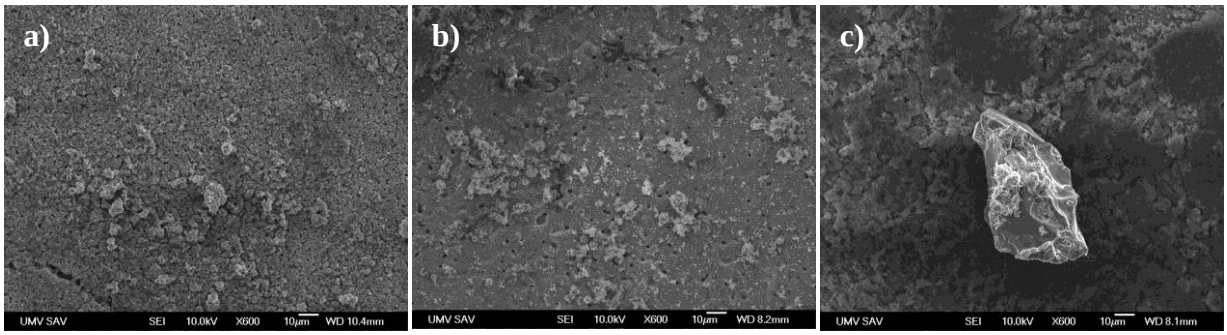

Figure 4. Electron microscopy observation of metal foam surfaces prepared by powder metallurgy after corrosion test in Hank's solution: Fe (a); Fe-CNTs (b); Fe-Mg (c).

The corrosion behaviour of Mg alloys is significantly dependent on the alloying elements and the microstructure [42]. As reported previously [43], the corrosion of Mg alloys initiated as localised corrosion. Mg alloys are susceptible to form a passivation layer of $Mg(OH)_2$ or a mixture of $Mg(OH)_2$

and MgO in aqueous solutions [44]. Due to the presence of chloride ions in physiological fluids, the protective coating may be destroyed and localized attack (i.e., pitting corrosion) initiates, which spread laterally and cover the whole surface. Thus localised corrosion in magnesium has an inherent tendency to be self-limiting. This is in marked contrast to the auto-catalytic pitting in stainless steels, where the occluded pit cell becomes more aggressive and accelerates the localised corrosion [43].

3.2.2 Physiological saline solution

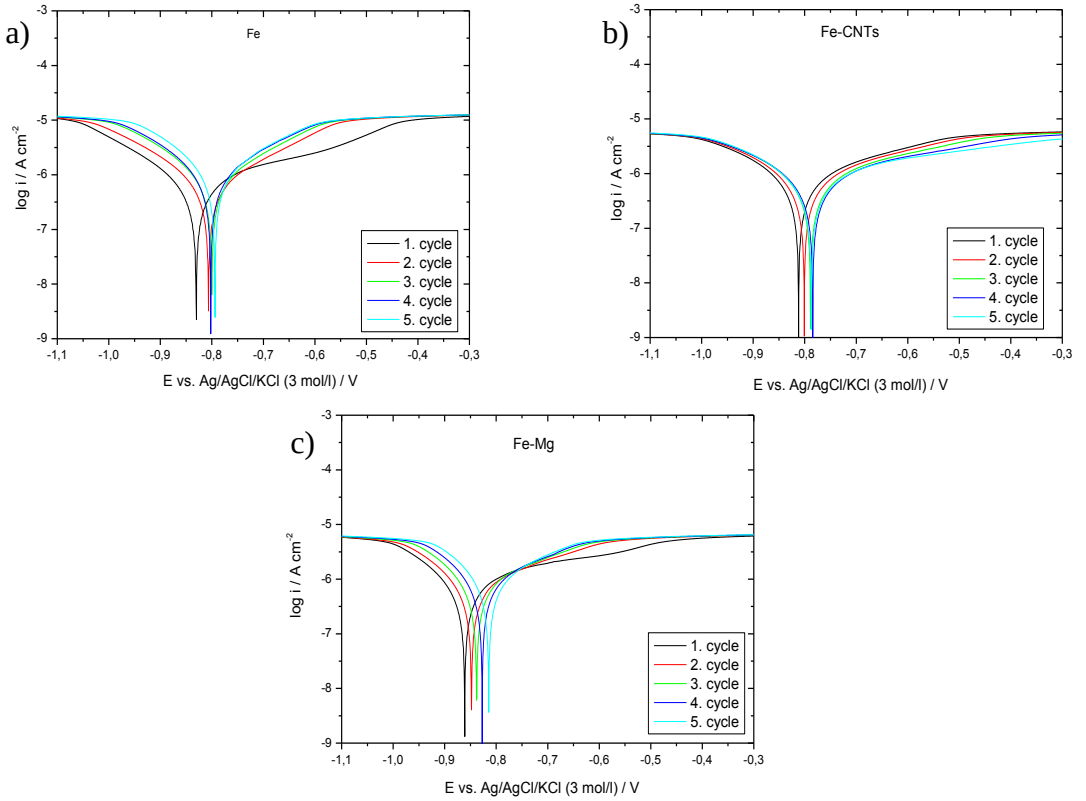

Figure 5. First five cycles of polarization curves of metal foams prepared by powder metallurgy in NaCl solution at pH 7.2 and 37°C: Fe (a); Fe-CNTs (b); Fe-Mg (c).

Degradation of iron foams was studied also in 9 g/l NaCl solution at 37°C. Five cycles of anodic potentiodynamic polarisation were again registered for every sample (Fig. 5). The values of E_{corr} and i_{corr} calculated from the intersection of the anodic and cathodic Tafel lines extrapolation together with the determined biodegradation rates for five cycles are summarized in Table 2.

The addition of CNTs caused shift of polarisation curves to less negative potential, though, addition of Mg resulted in opposite shift. This could be assigned to the high corrosion susceptibility of Mg in the presence of chloride anions. The shift of corrosion potential to the less negative values together with decrease in corrosion rate was observed for all experimental samples with increasing number of polarisation cycles indicating the passive layer formation. Again, the highest degradation rate was observed for Fe-Mg samples and lowest one for Fe-CNTs sample. The values of corrosion rate are higher than the values observed in Hank's solution due to the higher content of Cl^- ions. The

corrosion rate for Mg alloys is typically more than 1 mm/y in common testing solutions like 3% NaCl [39].

Table 2. Determined values of E_{corr}, i_{corr} and corrosion rates obtained from the potentiodynamic polarization curves in 9 g/l NaCl solution at pH 7.2 and 37°C.

Cycle	E_{corr} (mV)			i_{corr} (μA/cm^2)			Corrosion rate (mm/year)		
	Fe	Fe-CNTs	Fe-Mg	Fe	Fe-CNTs	Fe-Mg	Fe	Fe-CNTs	Fe-Mg
1.	-830.4	-811.4	-864.3	3.789	3.654	4.469	0.773	0.695	0.994
2.	-824.6	-795.2	-850.9	3.661	3.478	4.445	0.763	0.682	0.982
3.	-806.7	-782.9	-838.7	3.585	3.420	4.345	0.748	0.668	0.968
4.	-800.5	-780.3	-828.5	3.408	3.245	4.315	0.736	0.660	0.953
5.	-793.8	-783.0	-815.1	3.296	3.188	4.260	0.725	0.654	0.946

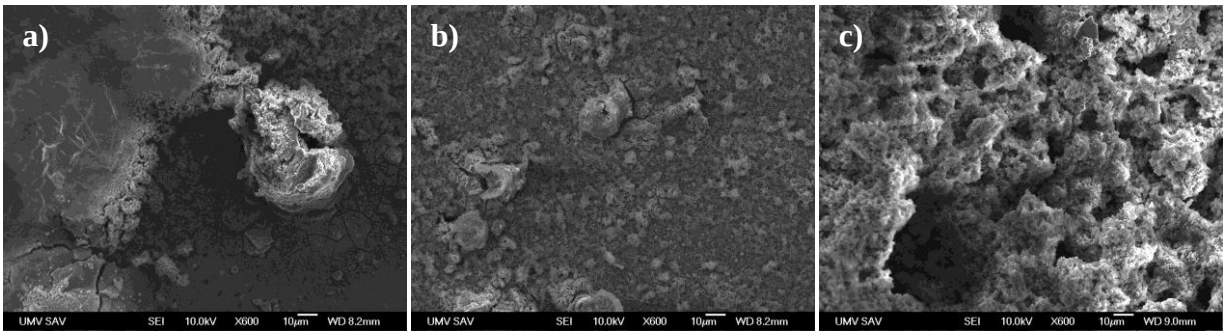

Figure 6. Electron microscopy observation of metal foam surfaces prepared by powder metallurgy after corrosion test in NaCl solution: Fe (a); Fe-CNTs (b); Fe-Mg (c).

The surface of corroded cellular material after corrosion test in NaCl solution is shown in Fig. 6. The amount of corrosion products on the surface is higher than that in Hank's solution. The extensive corrosion pits formation on the surface of bare iron sample was observed in contrast with the uniform corrosion of Fe-Mg sample. The highest amount of corrosion products together with highest extent of surface damage was again registered for Fe-Mg sample (Fig. 6c).

It was found by Atrens et al. [39], that the corrosion of Mg alloys in Hank's solution was only weakly influenced by the microstructure, in contrast to corrosion in 3% NaCl, where second phases cause strong micro-galvanic acceleration. This was attributed to the formation of a more protective surface film in Hank's solution, than in NaCl solution. Zhao et al. [43] have reported that a more negative corrosion potential; and a higher corrosion rate correlated with a higher chloride ion concentration in NaCl solution.

3.2.3 Mechanism of corrosion

The mechanism of corrosion of iron and its alloys in different media has been extensively discussed [24]. It is generally acknowledged that localized corrosion of iron occurs in Hank's solution [45].

A possible scheme of Fe anodic oxidation in chloride solution at pH ≥ 3 could be given by the following steps [46, 47]:

$$Fe + OH^- \Leftrightarrow FeOH_{ads} + e^- \quad (1)$$

$$FeOH_{ads} \rightarrow FeOH^+ + e^- \quad (2)$$

$$FeOH^+ \Leftrightarrow Fe^{2+} + OH^- \quad (3)$$

The first species formed on iron surface is $FeOH_{ads}$, which is independent of other anions added in the aqueous solution [46]. Ions Fe^{2+} and OH^- combine in solution to form iron (II) hydroxide which is further oxidized by dissolved oxygen [24]:

$$Fe + 2OH^- - 2e^- \rightarrow Fe(OH)_2 \quad (4)$$

$$4Fe(OH)_2 + O_2 \rightarrow 2Fe_2O_3.H_2O + 2H_2O \quad (5)$$

$$2Fe(OH)_2 + \frac{1}{2}O_2 + H_2O \rightarrow 2Fe(OH)_3 \quad (6)$$

Passive film breakdown could take place with the accumulation of chloride ions at the metal–solution interface [48]. After passive film breakdown any pits formed become covered by a loose corrosion product layer.

The following reactions were proposed as the second iron dissolution path in the presence of chloride ions, assuming that monovalent adsorbed species incorporating chloride ion are formed [47]:

$$Fe + Cl^- \rightarrow FeCl^-_{ads} \quad (7)$$

$$FeCl^-_{ads} \rightarrow FeCl_{ads} + e^- \quad (8)$$

$$Fe + Cl^- \rightarrow FeCl_{ads} + e^- \quad (9)$$

$$FeCl_{ads} \rightarrow FeCl^+ + e^- \quad (10)$$

$$FeCl^+ \Leftrightarrow Fe^{2+} + Cl^- \quad (11)$$

In physiological saline environment, Mg and its alloys degrade through the following electrochemical corrosion process [18, 1, 49]:

$$Mg + 2H_2O \rightarrow Mg(OH)_2 + H_2 \quad (12)$$

$$Mg + 2Cl^- \rightarrow MgCl_2 \quad (13)$$

$$Mg(OH)_2 + 2Cl^- \rightarrow MgCl_2 + 2OH^- \quad (14)$$

In the first reaction (12), gray $Mg(OH)_2$ film is developed on the surface of Mg as it reacts with water and hydrogen bubbles are also produced. The metal can also directly react with chloride ions to form Mg chloride (13). This highly soluble $MgCl_2$ is also formed through the reaction of $Mg(OH)_2$ with chloride ions, as depicted in (14) [18].

Reactions of metal cations (Fe^{2+}, Mg^{2+}) formed during anodic oxidation with other anions in Hank's solution could also take place:

$$M^{2+} + PO_4^{3-} \rightarrow M_3(PO_4)_2 \quad (M = Mg, Fe) \quad (15)$$

$$M^{2+} + CO_3^{2-} \rightarrow MCO_3 \quad (M = Mg, Fe) \quad (16)$$

3.3 Cytotoxicity studies

From the cytotoxicity results of it is obvious that all samples inhibited the viability of MC3T3 cells compared to that of Ti control. Fig. 7 illustrates the fluorescence microscopy images of osteoblasts adhered after 72 hours of incubation on: Ti (a); pure Fe (b); Fe-CNTs (c); and Fe-Mg (d) compacted pellet surfaces. The porous samples have also been tested, but the same or slightly higher inhibition of cells viability was observed.

The well adhered and spreaded osteoblast cells with numerous filopodia which mutually interconnected these cells can be seen on Ti sample surface indicating the very low cytotoxicity of control material (Fig. 7a). When the iron based experimental samples were used as substrates for osteoblast culturing, after 3 days, the cell densities significantly decreased on the surfaces of all three samples (Fig. 7c - d) compared to titanium control. The cell morphology changed to spherical shape without observable filopodia. Moreover, the small cell nuclei filled almost whole cell volumes. The decreased osteoblast densities on the iron based samples indicated the lower population growth and osteoblast proliferation and so the considerable cytotoxicity of samples. The compacts with CNTs (Fig. 7c), had the lowest osteoblast density. On the other hand, the cells on this substrate were most unfolded among three experimental samples.

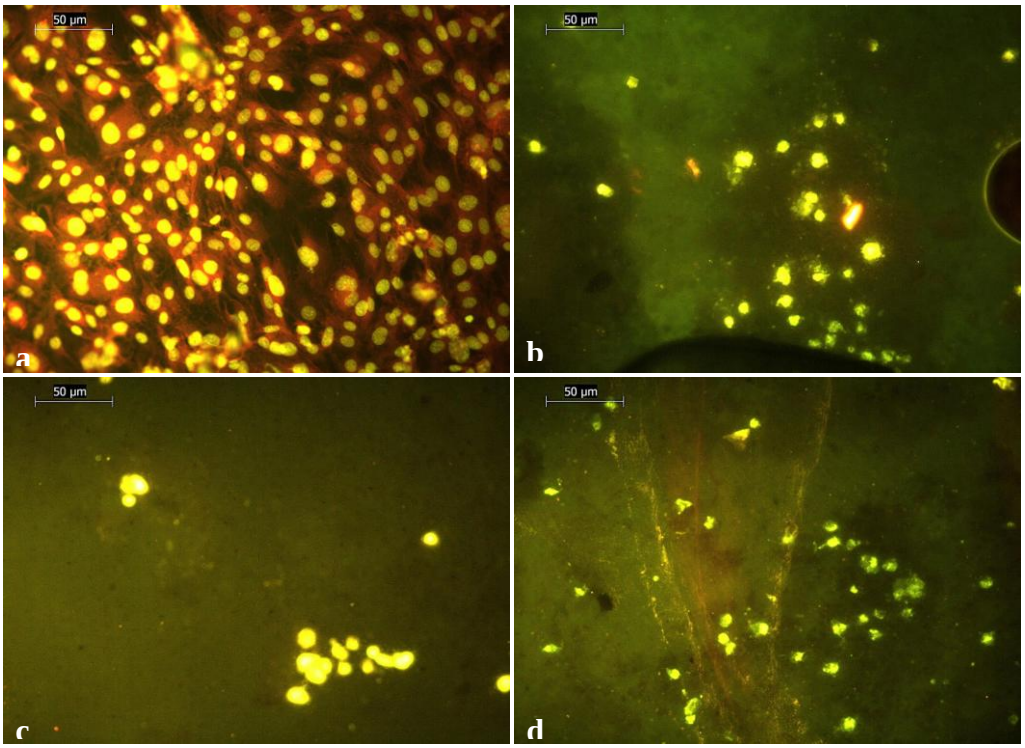

Figure 7. Fluorescence microscopy images of osteoblasts adhered after 72 hours of incubation on: Ti (a); pure Fe (b); Fe-CNTs (c); and Fe-Mg (d) compacted pellets surface.

No cytotoxicity to L929 and ECV304 cells was observed for pure Fe and Mg by Cheng [41]. The presence of magnesium was not significantly altered neither proliferation nor viability of U2OS

cells [50]. Furthermore, it was found that the Fe-CNT composite extracts induced no obvious cytotoxicity to L929 cells and ECV304 cells whereas significantly decreased cell viabilities of VSMC cells [37].

The massive corrosion of experimental samples during cytotoxicity test was observed. Degradation products resulting from the corrosion process probably inhibited the cells viability.

4. CONCLUSIONS

The iron based open cell foams were prepared by a powder metallurgical replication route. The addition of CNTs and Mg to the carbonyl iron powder on the in vitro electrochemical degradation and on the cytotoxicity of developed sintered cellular samples was investigated. The resulting material was characterized by microstructural analysis. It was found that the addition of CNTs and Mg resulted in higher surface roughness and positive shift of potentiodynamic polarisation curves in Hank's solution. Whereas for pure iron sample and sample containing CNTs the shift of corrosion potential to the less negative values accompanied with corrosion rate decrease was registered with increasing number of polarisation cycles, the opposite behaviour was observed for samples with magnesium. In NaCl solution, addition of CNTs caused shift of polarisation curves to less negative potential, but addition of Mg resulted in shift to more negative potential. Based on electrochemical data, it can be also found that the sequence of corrosion rate from high to low is: Fe-Mg, Fe, Fe-CNTs. Porous structure of sintered iron foams allowed increase in degradation rate. The localised corrosion was observed for bare iron sample and Fe-CNTs sample in contrast with the uniform corrosion of Fe-Mg sample.

The fluorescence observation of nuclei in MC3T3 cells showed significant change in morphology as well as viability inhibition of the cells incubated with iron based samples compared with a negative control. These results indicate the high amount of degradation product. Thus, the biocompatibility assessment should be conducted in a shorter period or in a dynamic system in order to anticipate the excessive accumulation of degradation products.

The open cell iron foams prepared by a powder metallurgical replication route seem to be a promising candidate for biodegradable materials in load bearing implants for orthopaedic applications. Nevertheless, further work on regulation the biocorrosion rate and reduction the cytotoxicity has to be done.

ACKNOWLEDGEMENTS
This work was supported by the Project APVV-0677-11 of the Slovak Research and Development Agency and Project VEGA 1/0211/12 of the Slovak Scientific Grant Agency.

References

1. Y.B. Wang, X.H. Xie, H.F. Li, X.L. Wang, M.Z. Zhao, E.W. Zhang, Y.J. Bai, Y.F. Zheng and L. Qin, *Acta Biomater.* 7 (2011) 3196
2. P. Tran and T.J. Webster, *Int. J. Nanomed.* 3 (2008) 391
3. B. Wegener, B. Sievers, S. Utzschneider, P. Müller,V. Jansson, S. Rößler, B. Nies, G. Stephani, B. Kieback and P. Quadbeck, *Mater. Sci. Eng. B* 176 (2011) 1789

4. H. Hermawan, D. Ramdan and J.R.P. Djuansjah, *Metals for Biomedical Applications, Biomedical Engineering - From Theory to Applications*, R. Fazel (Ed.), InTech. (2011)
5. A. Purnama, H. Hermawan, J. Couet and D. Mantovani, *Acta Biomater.* 6 (2010) 1800
6. G. Ryan, A. Pandit and D.P. Apatsidis, *Biomaterials* 27 (2006) 2651
7. T.J.Webster, L.S. Schadler, R.W. Siegel and R. Bizios, *Tissue Eng.* 7 (2001) 291
8. D.M. Robertson, L. Pierre and R. Chahal, *J. Biomed. Mater. Res.* 10 (1976) 335
9. H.N.G. Wadley, *Adv. Eng. Mater.* 4 (2002) 726
10. L.J. Gibson, *Annu. Rev. Mater. Sci.* 30 (2000) 191
11. P. Quadbeck, G. Stephani, K. Kümmel, J. Adler and G. Standke, *Mat. Sci. Forum* 534/536 (2007) 1005
12. G. Stephani, O. Andersen, H. Göhler, C. Kostmann, K. Kümmel, P. Quadbeck, M.Reinfried, T. Studnitzky and U. Waag, *Adv. Eng. Mater.* 8 (2006) 847
13. B. Liu, Y.F. Zheng and L. Ruan, *Mater. Lett.* 65 (2011) 540
14. N.J. Hallab, C. Vermes, C. Messina, K.A. Roebuck, T.T. Glant and C.C. Jacobs, *J. Biomed. Mater. Res.* 60 (2002) 420
15. R. Waksman, R. Pakala, R. Baffour, R. Seabron, D. Hellinga and F.O. Tio, *J. Interv. Cardiol.* 21 (2008) 15
16. M. Peuster, C. Fink, P. Wohlsein, M. Brügmann,A. Günther, V. Kaese, M Niemeyer, H. Haferkamp and C. Schnakenburg, *Biomaterials* 24 (2003) 393
17. M. Peuster, C. Hesse, T. Schloo, C. Fink, P. Beerbaum and C. von Schnakenburg, *Biomaterials* 27 (2006) 4955
18. A.H. Yusop, A.A. Bakir, N.A. Shaharom, M.R. Abdul Kadir and H. Hermawan, *Int. J. Biomater.* 2012 (2012) Article ID 641430, 10 pages
19. F. Witte, F. Feyerabend, P. Maier, J. Fischer, M. Störmer, C. Blawert, W. Dietzel and N. Hort, *Biomaterials* 28 (2007) 2163
20. Z.J. Li, X.N. Gu, S.Q. Lou and Y.F. Zheng, *Biomaterials* 29 (2008) 1329
21. C.M. Serre, M. Papillard, P. Chavassieux, J.C. Voegel and G. Boivin, *J. Biomed. Mater. Res.* 42 (1998) 626
22. C.E. Wen, M. Mabuchi, Y. Ymada, K. Shimojina, Y. Chino and T. Asahina, *Scr. Mater.* 45 (2001) 147
23. B. Heublein, R. Rohde, V. Kaese, M. Niemeyer, W. Hartung and A. Haverich, *Heart* 89 (2003) 651
24. B. Liu and Y.F. Zheng, *Acta Biomater.* 7 (2011) 1407
25. S. Aslan, M. Deneufchatel, S. Hashmi, N. Li, L.D. Pfefferle, M. Elimelech, E. Pauthe and P. R. Van Tassel, *J. Colloid Interf. Sci.* 388 (2012) 268
26. R. Oriňáková and A. Oriňák, *Fuel* 90 (2011) 3123
27. K. Sahithi, M. Swetha, K. Ramasamy, N. Srinivasan and N. Selvamurugan, *Int. J. Biol. Macromol.* 46 (2010) 281
28. M.D. Angione, R. Pilolli, S. Cotrone, M. Magliulo, A. Mallardi, G. Palazzo, L. Sabbatini, D. Fine, A. Dodabalapur, N. Cioffi and L. Torsi, *Mater. Today* 14 (2011) 424.
29. P.A. Tran, L. Zhang and T.J. Webster, *Adv. Drug Deliv. Rev.* 61 (2009) 1097
30. L.P. Zanello, B. Zhao, H. Hu and R.C. Haddon, *Nano Lett.* 6 (2006) 562
31. W. Tutak, K.H. Park, A. Vasilov, V. Starovoytov, G. Fanchini, S.Q. Cai, N.C. Partridge, F. Sesti and M. Chhowalla, *Nanotechnology* 20 (2009) 255101
32. S.B. Liu, A.K. Ng, R. Xu, J. Wei, C.M. Tan, Y.H. Yang and Y.A. Chen, *Nanoscale* 2 (2010) 2744
33. S. Kang, M. Pinault, L.D. Pfefferle and M. Elimelech, *Langmuir* 23 (2007) 8670
34. J.D. Schiffman and M. Elimelech, *ACS Appl. Mater. Interf.* 3 (2011) 462
35. B.A. Saw, Corrosion Resistance of Magnesium Alloys, *ASM Handbook*. 2003, 13
36. G. Song, A. Atrens, *Adv. Eng. Mater.* 5 (2003) 837
37. J. Cheng, Y.F. Zheng, *J. Biomed. Mater. Res. B*: *Appl. Biomater.* 101B (2013) 485

38. H. Sun, S. Liu and L. Sun, *Int. J. Electrochem. Sci.* 8 (2013) 3494
39. A. Atrens, M. Liu, N.I.Z. Abidin, *Mater. Sci. Eng. B* 176 (2011) 1609
40. H. Hermawan, H. Alamdari, D. Mantovani and D. Dube, *Powder Metall.* 51 (2008) 38
41. J. Cheng, B. Liu, Y.H. Wu, Y.F. Zheng, *J. Mater. Sci. Techno.,* 29 (2013) 619
42. W.M. Hosny, M.A. Ameer, *Int. J. Electrochem. Sci.* 8 (2013) 8371
43. M.C. Zhao, M. Liu, G.L. Song, A. Atrens, *Corros. Sci.* 50 (2008) 3168
44. H.B. Yao, Y. Li, A.T.S. Wee, *App. Surf. Sci.* 158 (2000) 112
45. G.S. Frankel and N. Sridhar, *Mater. Today* 11 (2008) 38
46. O.E. Barcia and O.R. Mattos, *Electrochim. Acta* 35 (1990) 1003
47. J.O'M. Bockris, D. Drazic and A.R. Despic, *Electrochim. Acta* 4 (1961) 325
48. N.J. Laycock and R.C. Newman, *Corros. Sci.* 39 (1997) 1771
49. M.P. Staiger, A M. Pietak, J. Huadmai and G. Dias, *Biomaterials* 27 (2006) 1728
50. Y.H. Yun, Z. Dong, D. Yang, M.J. Schulz, V.N. Shanov, S. Yarmolenko, Z. Xu, P. Kumta, C. Sfeir, *Mater. Sci. Eng. C* 29 (2009) 1814